ACS APPLIED NANO MATERIALS

www.acsanm.org Article

Substrate Lattice-Guided MoS_2 Crystal Growth: Implications for van der Waals Epitaxy

Yung-Yu Lai, Chi-Huang Chuang, Yen-Wei Yeh, Cheng-Hung Hou, Shih-Chieh Hsu, Yi Chou, Yi-Chia Chou, Hao-Chung Kuo, YewChung Sermon Wu, and Yuh-Jen Cheng*

Cite This: *ACS Appl. Nano Mater.* 2021, 4, 4930−4938 Read Online

ACCESS | Metrics & More | Article Recommendations | Supporting Information

ABSTRACT: Two-dimensional (2D) monolayer molybdenum disulfide (MoS_2) semiconductors are an emerging material with interesting device applications. MoS_2 crystals grown on a substrate often have random orientations due to weak van der Waals (vdW) interaction with the substrate. This leads to multiple grain boundaries when random orientated crystals coalesce. Understanding the conditions and mechanism to grow 2D crystals with an aligned orientation is crucial for high-quality single-crystal growth. Here, we study the introduction of oxidation etching in chemical vapor deposition to grow aligned MoS_2 crystals and elucidate the mechanism of the guided growth by a sapphire lattice through vdW interaction. Under proper oxygen flow conditions, single crystals are found to grow in two preferential orientations with triangle crystal edges aligned to the $[11\bar{2}0]$ or $[1\bar{1}00]$ direction of the sapphire substrate. These two orientations correspond to a superlattice of (3×3) MoS_2 on (2×2) sapphire and (5×5) MoS_2 on (3×3) sapphire and occur in Mo oxide- and sulfur-rich growth environments, respectively. This aligned orientation growth is realized by a carefully balanced etching and growth competition, which acts as a selection mechanism to grow energetically stable structures while etching less stable structures away. The commeasure of MoS_2 crystals with the sapphire lattice in the superlattice increases the bonding of MoS_2 to the sapphire lattice, thereby becoming the preferred stable structure for nucleation orientations. This study demonstrates the important role of etching−growth competition in the substrate lattice-guided 2D material growth and paves the way for the future development of vdW single-crystal epitaxy.

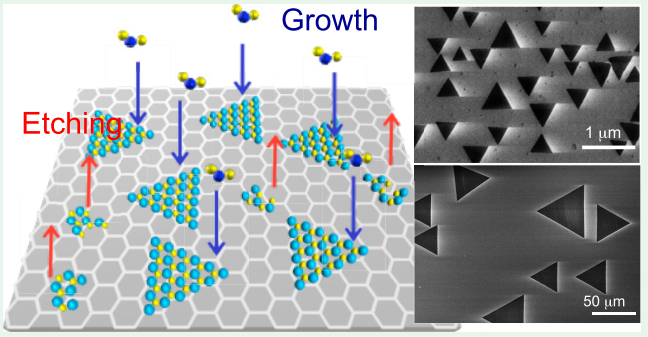

KEYWORDS: *two-dimensional materials, molybdenum disulfide (MoS_2), transition-metal dichalcogenides, chemical vapor deposition, crystal orientation, van der Waals epitaxy*

INTRODUCTION

Two-dimensional (2D) transition metal dichalcogenides (TMDCs) have unique physical and chemical properties, which open up interesting applications in next-generation electronics and optoelectronics. A direct bandgap monolayer TMDC semiconductor[1] can exhibit strong photoluminescence,[2] high optical responsivity,[3] spin valley polarization,[4,5] and strong light−matter interaction.[6,7] These unique properties have led to novel atomically thin device demonstrations, such as field-effect transistors,[8−10] sensors,[11] and photodetectors.[3,9] TMDC semiconductors also have high mechanical flexibility and mechanical breaking strength.[12] The above devices can in principle be built on flexible substrates.[13] Various methods have been developed to obtain monolayer TMDCs, including exfoliation from the bulk material,[14,15] physical vapor deposition,[16] chemical vapor deposition (CVD),[17−24] and metal−organic chemical vapor deposition (MOCVD).[25,26] Among them, CVD has attracted significant attention due to its simplicity in equipment setup and flexibility to scale up. MoS_2 is one of the most studied TMDCs due to its direct bandgap and strong photoluminescence property. There has been great interest to grow large-area MoS_2 by CVD using sulfur and MoO_3 precursors. Various techniques to assist crystal growth using salt promoters,[26−28] molten glass substrates,[28,29] and oxygen-assisted growth[30,31] have been reported. MoS_2 crystals grown on a substrate often have vast morphological variations due to inhomogeneous precursor distribution along the gas flow direction and the changes in MoO_3 vapor release caused by source poisoning. Grown crystals on a substrate very often show random orientations. When these crystal grains coalesce, they form grain boundary defects, which have negative effects on electron mobility and local optical properties.[32]

Received: February 14, 2021
Accepted: May 10, 2021
Published: May 19, 2021

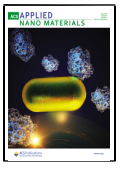

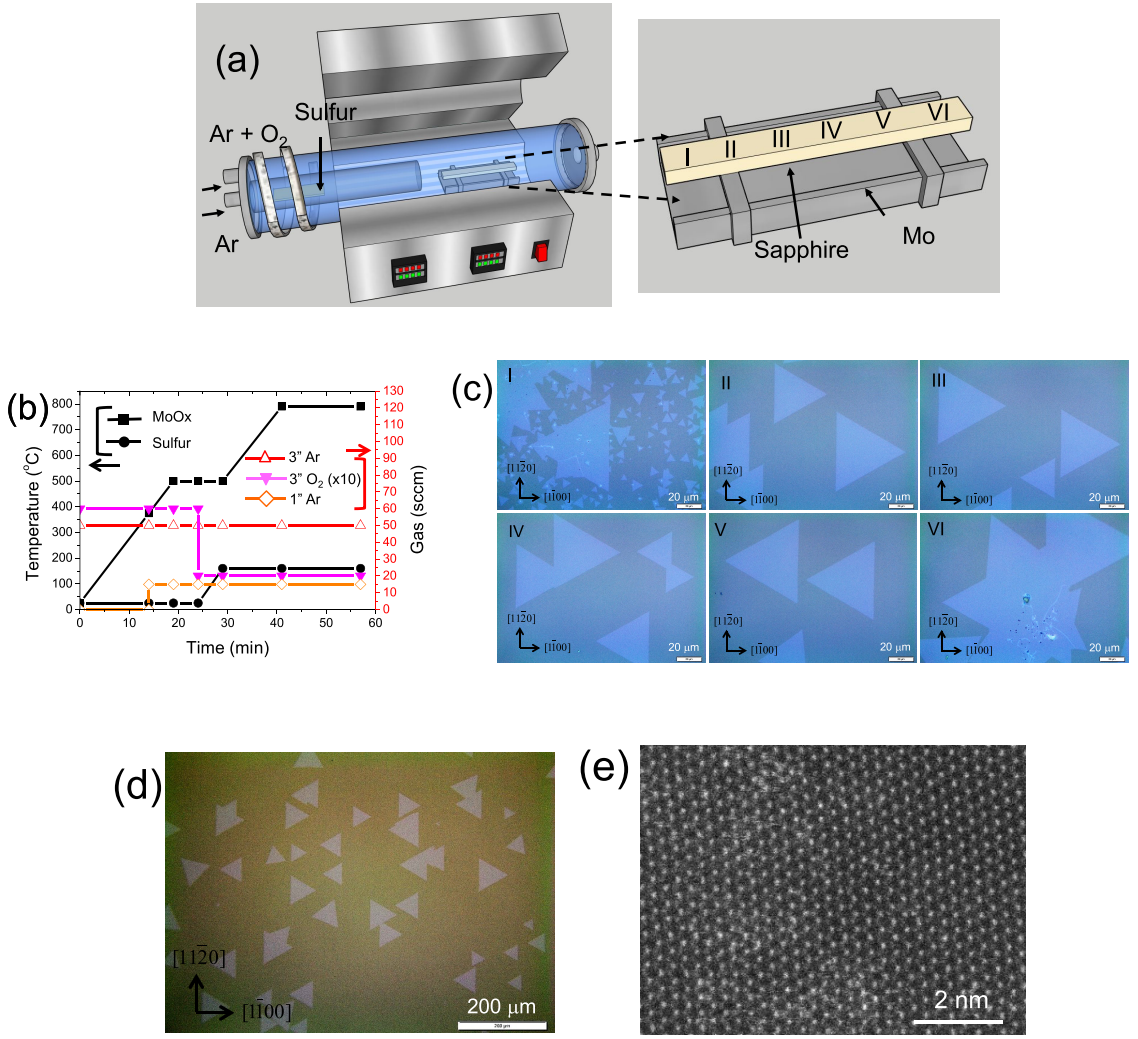

Figure 1. (a) Schematic of a CVD setup for MoS_2 growth. (b) Timeline profiles of gas flow and temperature at sulfur and substrate locations. (c) Optical microscope images at I–VI substrate locations, showing aligned triangle crystals with edges aligned to the [11$\bar{2}$0] direction. (d) Optical microscope image of a larger area showing the consistency of aligned crystals. (e) STEM image of grown MoS_2 crystals.

Recent research efforts have paid attention to the orientation of 2D crystals grown on a 3D material substrate.[33,34] The weak vdW interaction of a 2D material with a substrate without covalent bonds is considered beneficial for epitaxial growth because it relieves the need of a lattice-matched substrate as usually required for covalent 3D material epitaxy. However, lack of strong covalent bond guiding from the substrate lattice leads to random nucleation orientations, which form multiple grain boundaries when multiple nuclei grow and coalesce. Surprisingly, a recent statistical analysis of the orientation distribution of MoS_2 crystals grown on a *c*-plane sapphire substrate showed two broad peaks with triangle crystal edges aligned parallel to the [1$\bar{1}$00] and [11$\bar{2}$0] direction of the underlying sapphire substrate.[35] These two directions were shown by density functional theory calculations to be the minima in binding energy potential on the sapphire substrate. The potential minima are only a few tens of millielectronvolts lower than the highest-energy orientations.[35] This low energy barrier causes the broad orientation distribution. Later, Chen et al. reported an aligned growth guided by the step edge of sapphire.[36] Dumcenco et al. reported a narrow distribution of crystal orientations with triangle edges aligned solely to the [1$\bar{1}$00] direction of a sapphire substrate, wherein the key step was to anneal the sapphire substrate at 1000 °C for 1 h to prepare an atomically clean surface before growth.[37] Aljarb et al. also reported a narrow distribution in the same [1$\bar{1}$00] direction, where the key step is a high sulfur to MoO_3 ratio in the initial nucleation step using two-step growth temperature.[38] Suenaga et al. reported aligned crystal growth with triangle edges on the contrary aligned to [11$\bar{2}$0] at high sulfur concentration and [1$\bar{1}$00] at low sulfur concentration.[39] Wang et al. also reported an orientated crystal growth and suggested that a high growth temperature of ∼930 °C is the key to achieving an aligned orientation.[40] Interestingly, the aligned crystal growth can also occur on a GaN substrate, which has a very different lattice constant from sapphire.[41−43] These results indicate that 2D crystal growth with an aligned orientation can be achieved despite the weak vdW interaction with the substrate. The detail fundamental conditions and mechanisms leading to the aligned orientation, however, are still not clear and require further investigation.

Here, we introduce oxidation etching to investigate the growth condition and mechanism for aligned 2D crystal growth. Oxygen is introduced for two purposes. First, it is used to produce stable MoO_x vapor from oxidizing in situ molybdenum foil. In a typical CVD furnace, where sulfur

https://doi.org/10.1021/acsanm.1c00469
ACS Appl. Nano Mater. 2021, 4, 4930−4938

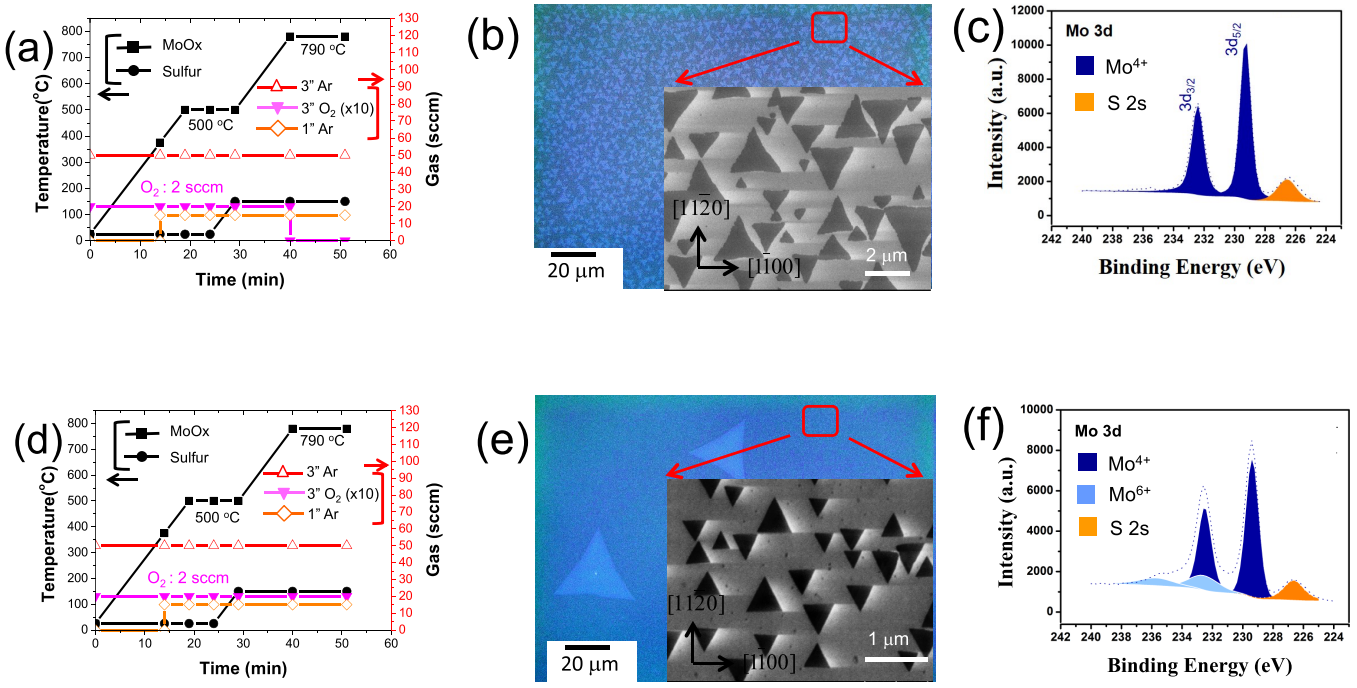

Figure 2. (a) CVD temperature and gas flow timeline profile, where oxygen flow is turned off after reaching a growth temperature of 790 °C. (b) Optical microscope image of grown MoS_2 crystals for the growth process (a). The inset is an SEM image. (c) XPS analysis showing that Mo foil is covered by MoS_2 after the growth process (a). (d) CVD temperature and gas flow timeline profile for continuous oxygen flow till the end of growth. (e) Optical microscope image of grown MoS_2 crystals for the growth process (d). The inset is an SEM image, showing an improved crystal structure and the aligned crystal orientations. (f) XPS analysis of Mo foil after growth showing that Mo foil is covered by MoS_2 and MoO_x after the growth process (d).

vapor reacts with the vapor generated from MoO_3 powder for a downstream MoS_2 growth, sulfurization also occurs on MoO_3 powder due to the exposure of MoO_3 power to sulfur vapor. As a result, MoS_2 forms on MoO_3 powder and hinders its continuous sublimation. The introduction of oxygen causes etching of MoS_2, which prevents the growth of capping MoS_2 on MoO_3 powder, thus ensuring a continuous MoO_x vapor release.[44,45] Second, oxygen causes etching to compete with the growth of MoS_2 on a sapphire substrate. A carefully adjusted oxygen flow can selectively etch away or prohibit the growth of unstable and defective MoS_2 while allowing an energetically stable crystal structure to grow. When the MoS_2 crystal is in an orientation commensurate with the sapphire lattice, the matched lattice registry enables a stronger vdW interaction with sapphire, thus becoming a more stable nucleation orientation that can survive etching and growth. We systematically adjust the oxygen flow condition to exploit this growth selection mechanism and find that there are two preferred growth orientations with triangle crystal edges respectively aligned to the $[1\bar{1}00]$ and $[11\bar{2}0]$ direction of the sapphire substrate. The detail oxygen tuning approach will be discussed. This study demonstrates that even though vdW interaction is a rather weak force, a properly adjusted etching–growth competition can enable a substrate lattice-guided vdW epitaxial growth.

RESULTS AND DISCUSSION

We introduce oxygen gas in the CVD process, where the gas-phase reaction of sulfur and MoO_x vapor is carried out in an Ar flow to grow MoS_2 on a sapphire substrate. Figure 1a schematically illustrates the CVD setup, which has a one-inch inner quartz tube to hold sulfur powder and a three-inch outer quartz tube to introduce oxygen gas. Ar is used as a carrier gas in both quartz tubes. Sulfur vapor was generated from sulfur powder heated at 160 °C and carried by Ar to react with MoO_3 downstream. Oxygen is introduced through an outer quartz tube to avoid reaction with sulfur. Instead of using MoO_3 powder as the solid MoO_x source, we choose to use oxygen to oxidize in situ Mo foil at 500 °C. A thin layer of Mo oxide is formed on Mo foil, which then sublimates to generate MoO_x vapor at temperature above 650 °C.[46] A *c*-plane sapphire substrate of 1 cm × 5 cm is placed face-down above the Mo foil. The substrate is diced from a 2″ diameter epi-ready grade substrate with a 1 cm side parallel to the sapphire *a*-plane $[11\bar{2}0]$ direction (Supporting Information S1). The substrate does not have any chemical or thermal pretreatment before growth as done in other aligned crystal growth studies.[37,38] Oxygen flow controls the extent of oxidation of Mo foil and therefore the generation of MoO_x for MoS_2 growth. The presence of oxygen at high temperature, on the other hand, also causes etching of MoS_2. Oxygen flow needs to be carefully controlled for the balance between etching, growth of MoS_2, and for the generation of MoO_x.

The optimized CVD heating and gas flow timeline profiles are shown in Figure 1b. Here, we mainly focus on the effect of the oxygen flow profile on MoS_2 growth. Growth details are provided in the Materials and Methods section. Temperature was intentionally held at 500 °C for 10 min to oxidize Mo foil before ramping up to the final growth temperature at 790 °C. Oxygen flow changes from 6 to 2 sccm at the 5th minute of the oxidation period. The first stage of 6 sccm oxygen flow produces MoO_x sourced from oxidizing Mo foil. The second stage of 2 sccm flow balances between the etching and growth of MoS_2. This CVD process grows perfect equilateral triangle

https://doi.org/10.1021/acsanm.1c00469
ACS Appl. Nano Mater. 2021, 4, 4930−4938

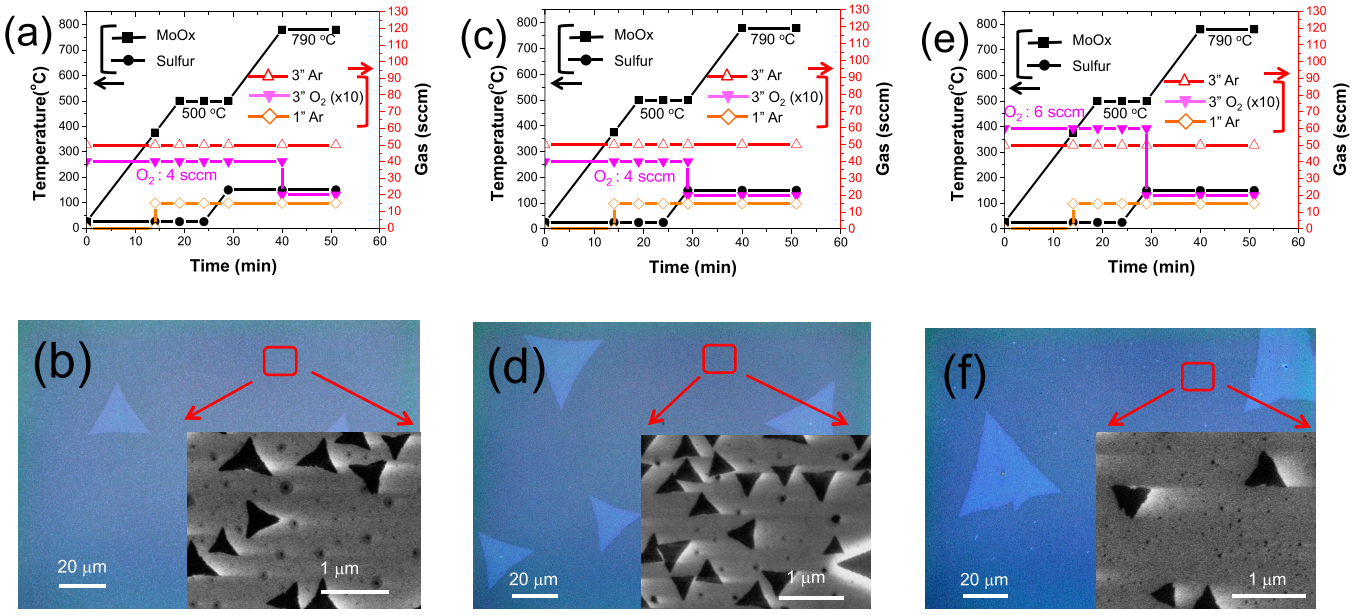

Figure 3. (a) Oxygen flow changing from 4 to 2 sccm at the start of the growth period (790 °C). (b) Crystals grown on the surface. (c) Oxygen flow changing from 4 to 2 sccm at the end of the oxidation period (500 °C). (d) Growth morphology with higher crystal density. (e) Starting oxygen flow increasing to 6 sccm while keeping the time changing to 2 sccm the same. (f) Crystal density decreasing with a slight increase in size.

MoS_2 crystals with crystal edges aligned to the $[11\bar{2}0]$ direction of the sapphire substrate, as shown in optical microscope (OM) images in Figure 1c taken at substrate positions I–VI depicted in the inset of Figure 1a. All the following image pictures were taken with the $[1\bar{1}00]$ direction of the sapphire substrate placed in the horizontal direction. The $[11\bar{2}0]$ direction of sapphire is accordingly in the vertical direction. Crystals grown near the edges of the substrate showed scattered distribution of orientations (Figure 1c (I, VI)). It is likely due to the change in the local growth environment at substrate edges. The optical microscope image in Figure 1d illustrates the consistency of crystal alignment over a larger area. This aligned crystal growth occurred over a nearly 4 cm length out of the total 5 cm length of the sapphire substrate. A continuous film can be achieved with an extended growth time of 50 min (Supporting Information, Figure S2a). XPS analysis of single crystals in Figure 1c shows the composition in a near perfect Mo:S = 1:2 ratio (Supporting Information, Figure S2b). The matching of Mo foil length to the sapphire length is helpful to achieve this orientation uniformity over a large area. A scanning tunneling electron microscope image of grown MoS_2 crystals is shown in Figure 1f, showing a crystalline atomic symmetry structure.

The oxygen flow profile plays an important role to realize this aligned crystal growth. It produces in situ MoO_x and at the same time introduces etching to compete with the growth of MoS_2. When these two counteracting processes are properly balanced, it selectively grows crystal structures that are energetically stable on the substrate and etches away less energetically stable crystal defects or structures, thereby improving overall grown crystal quality. The near perfect equilateral triangle shape is an indication of good crystalline growth.[20,37,40] The two-stage oxygen flow profile was systematically developed through a sequence of heuristic trials and adjustments. We have explored various growth parameters. A few key trials are described in the following to shed light on the tuning approach taken to reach this two-stage flow profile.

We first tested an oxygen flow profile, where the oxygen flow rate was set at 2 sccm and turned off when the furnace reached growth temperature (Figure 2a). Small and dense triangle crystals of ~1–2 μm size were grown on a sapphire substrate, as shown in Figure 2b. The inset in Figure 2b is a magnified scanning electron microscope (SEM) image, showing triangle crystals with slight distortion. It is very special that all crystals are aligned with their edges parallel to the $[1\bar{1}00]$ direction of the sapphire substrate. The surface composition of Mo foil after growth was analyzed by X-ray photoelectron spectroscopy (XPS), where we specifically looked for the binding states related to MoO_x and MoS_2. XPS analysis showed that the Mo foil surface was largely covered by MoS_2 at the end of the growth process (Figure 2c) (Supporting Information, Figures S3c and S4c). This indicates that sulfur vapor, while reacting with MoO_x vapor to grow MoS_2 on the sapphire substrate, also sulfurized solid MoO_x on Mo foil and formed a capping MoS_2 layer. This MoS_2 capping layer hindered the continuous sublimation of MoO_x and eventually stopped the crystal growth. The growth condition is expected to be in a relatively sulfur-rich condition due to this decrease in MoO_x vapor release. We tried another growth run with oxygen flow kept at 2 sccm till the end of growth (Figure 2d). The presence of oxygen during the crystal growth period changed the growth morphology to a dense distribution of submicrocrystals with occasional sparse crystals of ~20 μm size (Figure 2e). We took a closer look at the substrate surface using an SEM. Interestingly, there were near perfect equilateral triangle crystals of 0.2–0.5 μm size densely distributed across the whole area (Figure 2e inset). These small crystals were near 100% aligned with their edges parallel to the $[1\bar{1}00]$ direction of the sapphire substrate. The small size allowed crystals to rotate into an orientation commensurate with the sapphire lattice, which strengthened interfacial vdW bonding to the sapphire lattice[43] and locked down the orientation. These aligned crystals cover most of the substrate area except near substrate edges (Supporting Information, Figure S5). Sparse large MoS_2 often has a seed particle at the center, as shown by

https://doi.org/10.1021/acsanm.1c00469
ACS Appl. Nano Mater. 2021, 4, 4930–4938

the tiny white dot at the center of large crystals in Figure 2e. This particle is a sulfurized MoO_x particle (multiple-layer MoS_2)[38] landed on the sapphire surface from the MoO_x source. It initiates nucleation early and grows into a large crystal. The seed particle, however, does not guide the crystal growth orientation, leading to random orientations. For small crystals, growth starts from MoS_2 spontaneous nucleation guided by the substrate lattice, thus leading to aligned crystal growth. It takes time to aggregate Mo and S from the precursor to start nucleation and therefore leads to small crystal size due to shorter growth time. XPS analysis of Mo foil after growth showed the presence of Mo^{6+} and Mo^{4+} along with the S signal, indicating that both MoS_2 and MoO_x were present on the Mo foil surface at the end of the growth process (Figure 2f) (Supporting Information, Figures S3b and S4b). The presence of oxygen caused oxidation etching of MoS_2, which prevented the formation of a continuous capping MoS_2 layer on Mo foil. Both MoS_2 and MoO_x were thus present on the Mo foil surface. The presence of oxidation etching also competes with the growth of MoS_2 on sapphire. Under proper conditions, it selectively etches away energetically unstable crystal defects while letting stable crystal structures grow. This leads to the near perfect equilateral triangle crystal growth, as shown in the inset of Figure 2e, in sharp contrast to the distorted triangles in the inset of Figure 2b. A side effect of this improved growth is a reduced grown crystal size due to etching.

We have tried different oxygen flow values. A higher oxygen flow caused etching to overtake growth and resulted in no crystal growth. A lower oxygen flow on the other hand caused source poisoning, which resulted in defective crystal growth similar to that shown in Figure 2b. These observations indicate that introducing oxygen flow not only prevents source poisoning but also improves crystal growth quality through etching and growth competition, as shown by the improved triangle shape. Interestingly, it also leads to crystal growth with an aligned orientation.

To have independent control on MoO_x production and oxidation etching, we introduce a two-step oxygen flow in the growth process: one flow rate for producing MoO_x before reaching growth temperature and one for controlling the balance between etching and growth of crystals at growth temperature. We first increased the starting oxygen flow to 4 sccm to produce more MoO_x from Mo foil and switched to 2 sccm when the furnace reached growth temperature, as shown by the oxygen flow timeline profile in Figure 3a. Sparse crystals of 30−40 μm size were still present on the sapphire surface (Figure 3b). The rest of the open area was covered by small crystals with a random orientation (Figure 3b inset SEM image). The morphology change is attributed to the increase in MoO_x supply and delayed response time of the gas flow change. When oxygen flow changed from 4 to 2 sccm, it took a certain time for the oxygen environment to settle from the 4 to 2 sccm condition. The 4 sccm oxygen flow produces more MoO_x, but the delayed response time for the flow change caused an excess oxygen environment and thus higher oxidation etching at the beginning of the growth period (790 °C region). The overetching mostly affects the small crystal growth, leading to a distorted shape.

Taking this delayed response into consideration, we moved the 4 to 2 sccm oxygen flow change ahead by 10 min to where temperature started to ramp up from 500 °C (Figure 3c). This in advance flow change allowed oxygen flow in the furnace to have more time to decay toward the 2 sccm condition as the furnace reached growth temperature. Previous high oxidation etching caused by the delayed oxygen flow change was reduced. As a result, grown crystals showed an increase in nucleation density (Figure 3d). To increase MoO_x supply, we tried another growth run with the initial oxygen flow increased to 6 sccm while keeping the time switching to 2 sccm the same (Figure 3e). The grown crystals shown in Figure 3f, as compared with the previous case (Figure 3d), showed a decrease in nucleation density and a slight increase in size. The higher initial 6 sccm oxygen flow produced more MoO_x, though it required a longer time to settle to the 2 sccm condition. This longer settling time again caused an increase in oxidation etching during growth. As a result, it decreased nucleation density, in particular for the small crystals, as they were more susceptible to etching. A seed particle is present at the center of large misaligned crystals, which is a sulfurized MoO_x particle caused by the oversupply of MoO_x. It starts crystal growth without orientation control, leading to random crystal orientations.

To reduce this oxidation etching, we moved the 6 to 2 sccm change further ahead into the middle of the 500 °C oxidation time period, as shown by the timeline profile of oxygen flow in Figure 1b. This allowed more time for oxygen flow to decay toward 2 sccm when the furnace reached growth temperature. This carefully adjusted oxygen flow profile led to an increase in nucleation density for large crystals as seen by comparing Figure 1c,d to Figure 3f, while there was no small crystal grown on the surface, which is probably because the precursor was used up by the growth of large crystals leaving no room for small crystals to nucleate and grow. These large crystals showed perfect equilateral triangle shapes with size up to 80 μm. There is no seed particle at the center of large crystals due to no MoO_x oversupply, as compared with the case in Figure 3f. Growth now starts from MoS_2 spontaneous nucleation guided by the substrate lattice, thus leading to aligned crystal growth. Interestingly, these large crystals were all well-aligned with edges parallel to the $[11\bar{2}0]$ direction of the underlying sapphire substrate. This is in sharp contrast to the case shown in Figure 2e, where small crystals in the size of submicrometers were aligned with edges parallel to the $[1\bar{1}00]$ direction of the sapphire substrate. The growth condition difference between those aligned to the $[11\bar{2}0]$ and $[1\bar{1}00]$ direction is merely the oxygen flow profile: the former one using a 6 to 2 sccm two-step (Figure 1b) and the latter one using a 2 sccm continuous oxygen flow (Figure 2d). The former case has more MoO_x supply than the latter one. The growth conditions for these two orientations are thus identified to be MoO_x- and sulfur-rich conditions, respectively.

The presence of oxygen flow introduces etching to compete with growth. From the above careful tuning of oxygen flow, it leads to two preferred growth orientations aligned to the $[11\bar{2}0]$ and $[1\bar{1}00]$ directions of the sapphire substrate. To explain these preferential orientations, density functional theory has been used to calculate the binding potential of the vdW interaction between MoS_2 and sapphire. Some reports show that the local energy minimum occurs only in the $[1\bar{1}00]$ direction[37,38] and some reports in both $[1\bar{1}00]$ and $[11\bar{2}0]$ directions.[35,39] This discrepancy could be due to different modeling details in each report. Here, we elucidate these two stable orientations from a crystallographic viewpoint. In heteroepitaxial growth, a crystal tends to grow in an orientation with its lattice commensurate with the underlying substrate due to better nucleation stability. The periodicity of the

https://doi.org/10.1021/acsanm.1c00469
ACS Appl. Nano Mater. 2021, 4, 4930−4938

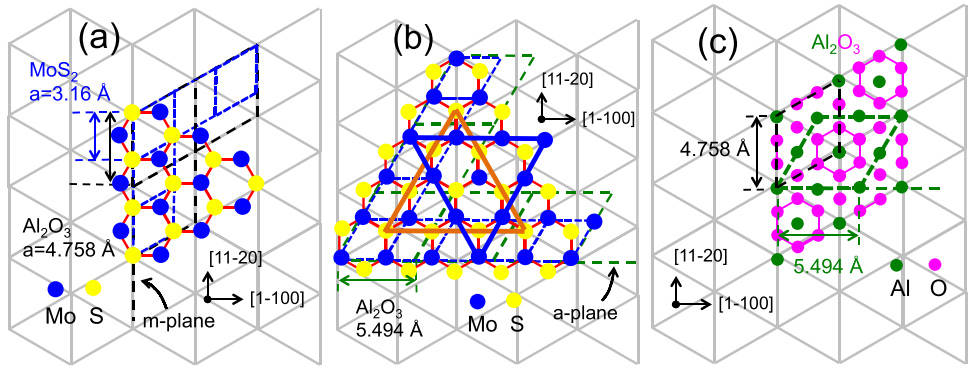

Figure 4. MoS_2 crystal structure on sapphire. (a) MoS_2 triangle edge aligned to the $[11\bar{2}0]$ direction (parallel to the *m*-plane) of sapphire. It forms a superlattice of the (3×3) MoS_2 dashed blue unit cell on the (2×2) sapphire dashed black unit cell. (b) MoS_2 triangle edge aligned to the $[1\bar{1}00]$ direction (parallel to the *a*-plane) of sapphire. It forms a superlattice of the (5×5) MoS_2 dashed blue unit cell on the (3×3) sapphire dotted green unit cell. (c) Sapphire unit cell represented by a dashed black parallelogram formed by *m*-plane lines and the dashed green parallelogram formed by *a*-plane lines.

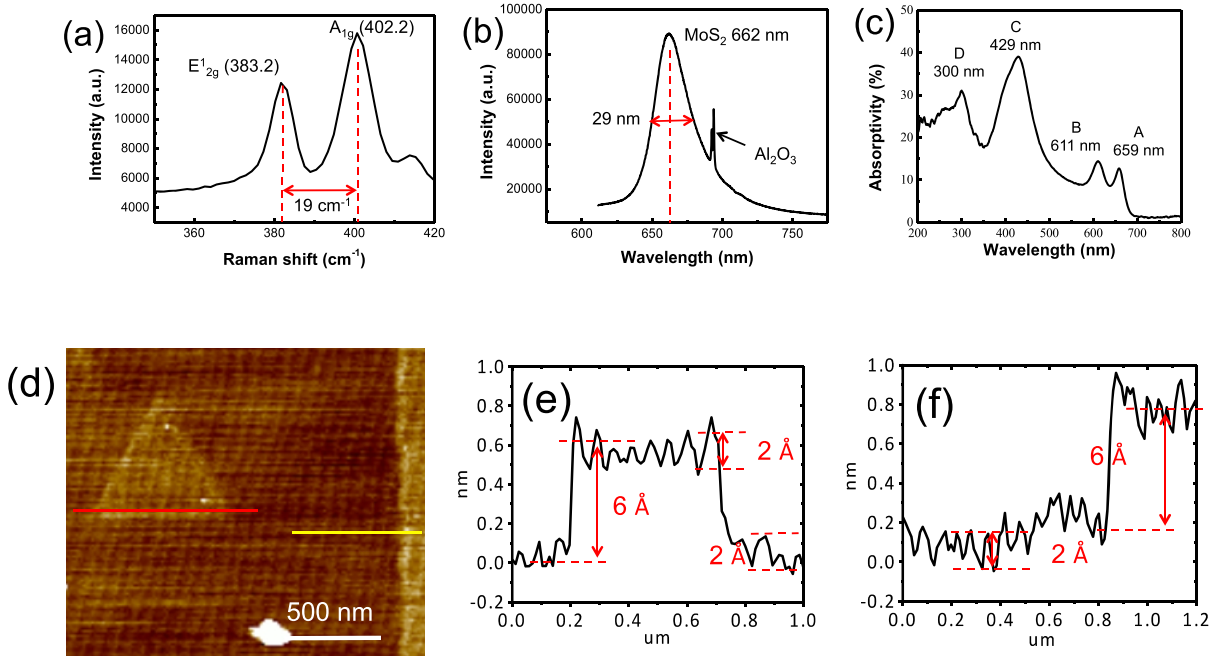

Figure 5. (a) Raman spectrum of as-grown MoS_2 crystals. A peak separation of 19 cm^{-1} indicates a monolayer. (b) Photoluminescence spectrum of as-grown MoS_2 crystals. (c) Absorption spectrum showing A and B band edge exciton absorption and the higher-energy C and D excitonic absorption by the van Hove singularities of the MoS_2 monolayer. (d) AFM image of small MoS_2 crystals in Figure 2e. A white dashed line indicates the direction of fine sapphire terrace step edges. (e) Surface profile of MoS_2 crystals depicted by the red line in (d). (f) Surface profile of MoS_2 crystals depicted by the yellow line in (d).

sapphire lattice (4.758 Å) is 1.506 times of the MoS_2 lattice constant (3.16 Å). When the triangle edge of the MoS_2 crystal is aligned to the $[11\bar{2}0]$ direction (parallel to the *m*-plane of sapphire), as shown in Figure 4a, it forms a coincident superlattice of (3×3) MoS_2 on (2×2) sapphire as illustrated by the MoS_2 and sapphire unit cells depicted by dashed blue and black parallelograms. In this orientation, there is a 0.4% tensile strain in MoS_2, which can be elastically accommodated. When the triangle edge of the MoS_2 crystal is aligned to the $[1\bar{1}00]$ direction (parallel to the *a*-plane), it forms a superlattice of (5×5) MoS_2 on (3×3) sapphire, as shown in Figure 4b. To visualize this latter superlattice, the original sapphire unit cell depicted by a dashed black parallelogram is replaced by the dashed green parallelogram formed by the *a*-plane lines, as illustrated in Figure 4c. The lattice constant of this unit cell is 5.494 Å. It is very close to a 5 to 3 ratio with respect to the MoS_2 lattice constant, which leads to a superlattice of (5×5) MoS_2 on (3×3) sapphire as illustrated in Figure 4b. The estimated tensile strain is 4% in this orientation. The commeasure of the MoS_2 lattice with the sapphire lattice in these two orientations allows vdW interaction to increase MoS_2 bonding and therefore nucleation stability on a sapphire substrate. This interaction force, however, provides only a few tens of millielectronvolts of binding energy according to density functional theory calculation.[35] It therefore requires a carefully balanced etching−growth condition to realize such an orientation-selective growth. In the current study, aligned crystal growth often occurs in one of the two orientations depending on growth conditions. They do not occur in both orientations simultaneously. This suggests that in addition to

https://doi.org/10.1021/acsanm.1c00469
ACS Appl. Nano Mater. 2021, 4, 4930−4938

commensuration with the substrate lattice, the growth condition also plays an important role in choosing one of the two orientations. It has been reported that termination of MoS_2 crystals depends on the growth environment. A Mo (S)-rich growth environment results in Mo (S)-terminated triangle MoS_2 crystals.[20] The MoS_2 crystal in Figure 4a and 4b is thus drawn with Mo and S termination, respectively. It is worth noting that one can draw both S- and Mo-terminated triangles (orange and blue triangles) in Figure 4b (likewise Figure 4a) with two triangles in 60° rotation with respect to each other. In other words, both terminations have the same lattice registry commensurate with the sapphire lattice. Termination is therefore not likely a reason for choosing the orientation in Figure 4a or b. Since the orientation depends on precursor conditions, the selection is therefore attributed to a precursor-dependent sapphire surface modification that promotes a specific growth orientation.

To verify the MoS_2 crystal quality, we measured Raman, photoluminescence, and absorption spectra using samples in Figure 1c. Figure 5a shows two typical Raman peaks. One corresponds to an out-of-plane vibration mode with a Raman shift of 402.2 cm^{-1}, and the other corresponds to an in-plane vibration mode with a Raman shift of 383.2 cm^{-1}. The Raman shift difference of 19 cm^{-1} confirms the monolayer of grown MoS_2 crystals. Figure 5b is a typical photoluminescence spectrum. It shows a strong A exciton peak at 662 nm with a full width at half maximum linewidth of 29 nm. This relatively narrow linewidth indicates good crystal quality.[37] Figure 5c shows the absorption spectrum. It shows the well-known A and B excitonic absorption peaks by band edge excitons.[2,46] In addition, it also shows the higher-energy C and D excitonic absorption by the van Hove singularities of the MoS_2 monolayer.[1] These observations indicate a decent optical property of the grown MoS_2 crystals. Figure 5d is the AFM image of MoS_2 crystals grown with continuous 2 sccm oxygen flow shown in Figure 2e. The edges of small crystals are all aligned to the $[1\bar{1}00]$ direction. Figure 5e is a surface line scan profile over a crystal depicted by a red line in Figure 5e. The layer thickness of 6 Å indicates a monolayer MoS_2 crystal. The fine stripes on the whole surface are the sapphire terrace steps due to an ∼0.2° off-cut angle of the sapphire surface with respect to the sapphire *c*-axis. The step edge height is about 2 Å, and the terrace width is about 80 nm.[47,48] The terrace step height is much smaller than MoS_2 thickness and does not affect MoS_2 growth at all. Interestingly, sapphire terrace step morphology is also shown on the MoS_2 surface, as indicated by the ripples on MoS_2 in Figure 5e. The reduced corrugation depth at the center indicates that the MoS_2 film is slightly stretched over sapphire terrace steps. These corrugations suggest that MoS_2 is flexible enough to grow over and follow the step edge corrugation. This AFM image was intentionally taken near an occasionally occurred large crystal, which is shown on the right in the figure. The edge of this large crystal depicted by a blue line is aligned to the sapphire $[11\bar{2}0]$ direction. Figure 5f is an AFM surface line scan (yellow line in Figure 5d) showing monolayer thickness and a similar corrugated surface feature. These AFM surface analyses show that the MoS_2 crystal orientation is guided by the sapphire crystal lattice and independent of its surface step edges.

CONCLUSIONS

In conclusion, we have demonstrated a highly aligned MoS_2 crystal growth by introducing oxygen in the CVD growth process. Oxygen flow causes oxidation etching to compete with the growth of MoS_2. Through careful tuning, the balance between etching and growth leads to a selective growth of energetically stable crystal structures. This selection mechanism leads to aligned orientation growth with triangle crystal edges aligned to the $[11\bar{2}0]$ and $[1\bar{1}00]$ directions of the sapphire substrate. These two orientations respectively correspond to a superlattice of (3×3) MoS_2 on (2×2) sapphire and (5×5) MoS_2 on (3×3) sapphire. They are identified to occur under MoO_x- and sulfur-rich growth conditions, respectively. The commeasure of the lattice structure allows the vdW interaction with the sapphire surface to stabilize MoS_2 nucleation and therefore promotes crystal growth in these two orientations. Due to the weak vdW interaction, it requires a carefully balanced etching−growth competition to realize such an orientation-selective growth. This selective growth process and the understanding of mechanisms are important for the future development of large-scale single MoS_2 crystal growth. The approach can also be applied to other 2D materials grown on a crystalline substrate.

MATERIALS AND METHODS

Growth Procedure. The MoS_2 crystal was grown on a *c*-plane sapphire substrate by chemical vapor deposition (CVD). The furnace had a one-inch quartz tube inside a three-inch quartz tube. Sulfur powder (Sigma-Aldrich, ≥99.9% purity) was placed in the one-inch tube heated at 160 °C to generate sulfur vapor. Oxygen (2−6 sccm) and Ar (50 sccm) were introduced to the outer three-inch quartz tube to oxidize Mo foil (Sigma-Aldrich, ≥99.9% purity) placed at the reaction zone to generate MoO_x vapor. Sulfur vapor was carried by Ar (15 sccm) downstream to react with MoO_x vapor. A *c*-plane sapphire substrate was placed face-down above the Mo foil. The furnace temperature was first raised to 500 °C from room temperature at a 25 °C/min ramping rate, maintained at 500 °C for 10 min, and then raised to a growth temperature of 790 °C at the same ramping rate and maintained for 10 min. The furnace cooled down naturally after growth. Sulfur temperature was raised to 160 °C at a 25 °C/min ramping rate. It reached 160 °C at the same time when the furnace temperature started ramping up from 500 °C.

Characterization. Optical microscope images were taken using an Olympus BX51. Scanning electron microscopy images of MoS_2 crystals on sapphire were taken using a Hitachi SU-8010 without precoating of a conductive layer. Due to the nonconductive nature of the sapphire substrate, images had to be taken as soon as possible before charging caused image distortion. Both Raman spectroscopy and photoluminescence spectroscopy were performed using an Andor SR500 with 532 nm laser excitation. Atomic force microscope images were taken using a Bruker Dimension Icon using tapping mode. XPS spectra were acquired using a PHI 5000 VersaProbe (ULVAC-PHI, Japan) system using a monochromatic Al Kα X-ray beam with a beam diameter of 100 μm. An electron beam and an Ar+ beam, both with acceleration voltages of 10 V, were applied on the surface to compensate for the surface charge during spectrum acquisition processes.

ASSOCIATED CONTENT

Supporting Information

The Supporting Information is available free of charge at https://pubs.acs.org/doi/10.1021/acsanm.1c00469.

Sapphire substrate orientation, XPS analysis, and supplementary SEM images of aligned MoS_2 crystal growth (PDF)

https://doi.org/10.1021/acsanm.1c00469
ACS Appl. Nano Mater. 2021, 4, 4930−4938

AUTHOR INFORMATION

Corresponding Author

Yuh-Jen Cheng − *Research Center for Applied Sciences, Academia Sinica, Taipei 115, Taiwan; Department of Photonics and Institute of Electro-Optical Engineering, National Chiao Tung University, Hsinchu 300, Taiwan;* orcid.org/0000-0002-0575-4296; Email: yjcheng@sinica.edu.tw

Authors

Yung-Yu Lai − *Department of Materials Science and Engineering, National Chiao Tung University, Hsinchu 300, Taiwan*

Chi-Huang Chuang − *Research Center for Applied Sciences, Academia Sinica, Taipei 115, Taiwan*

Yen-Wei Yeh − *Department of Photonics and Institute of Electro-Optical Engineering, National Chiao Tung University, Hsinchu 300, Taiwan*

Cheng-Hung Hou − *Research Center for Applied Sciences, Academia Sinica, Taipei 115, Taiwan;* orcid.org/0000-0002-5150-7106

Shih-Chieh Hsu − *Department of Chemical and Materials Engineering, Tamkang University, New Taipei City 25137, Taiwan;* orcid.org/0000-0001-9142-114X

Yi Chou − *Department of Electrophysics, National Chiao Tung University, Hsinchu 300, Taiwan*

Yi-Chia Chou − *Department of Electrophysics, National Chiao Tung University, Hsinchu 300, Taiwan;* orcid.org/0000-0002-7775-2927

Hao-Chung Kuo − *Department of Photonics and Institute of Electro-Optical Engineering, National Chiao Tung University, Hsinchu 300, Taiwan*

YewChung Sermon Wu − *Department of Materials Science and Engineering, National Chiao Tung University, Hsinchu 300, Taiwan*

Complete contact information is available at: https://pubs.acs.org/10.1021/acsanm.1c00469

Notes

The authors declare no competing financial interest.

ACKNOWLEDGMENTS

The authors acknowledge financial support from the Academia Sinica, Taiwan, under grant AS-iMATE-110-42, and the Ministry of Science and Technology, Taiwan, under grant MOST 108-3116-F-008-005.

REFERENCES

(1) Mak, K. F.; Lee, C.; Hone, J.; Shan, J.; Heinz, T. F. Atomically Thin MoS2: A New Direct-Gap Semiconductor. *Phys. Rev. Lett.* **2010**, *105*, 136805.

(2) Splendiani, A.; Sun, L.; Zhang, Y.; Li, T.; Kim, J.; Chim, C. Y.; Galli, G.; Wang, F. Emerging Photoluminescence in Monolayer MoS_2. *Nano Lett.* **2010**, *10*, 1271−1275.

(3) Lopez-Sanchez, O.; Lembke, D.; Kayci, M.; Radenovic, A.; Kis, A. Ultrasensitive Photodetectors Based on Monolayer MoS_2. *Nat. Nanotechnol.* **2013**, *8*, 497−501.

(4) Zeng, H.; Dai, J.; Yao, W.; Xiao, D.; Cui, X. Valley Polarization in MoS_2 Monolayers by Optical Pumping. *Nat. Nanotechnol.* **2012**, *7*, 490−493.

(5) Saito, Y.; Nakamura, Y.; Bahramy, M. S.; Kohama, Y.; Ye, J.; Kasahara, Y.; Nakagawa, Y.; Onga, M.; Tokunaga, M.; Nojima, T.; Yanase, Y.; Iwasa, Y. Superconductivity Protected by Spin−Valley Locking in Ion-Gated MoS_2. *Nat. Phys.* **2016**, *12*, 144−149.

(6) Britnell, L.; Ribeiro, R. M.; Eckmann, A.; Jalil, R.; Belle, B. D.; Mishchenko, A.; Kim, Y.-J.; Gorbachev, R. V.; Georgiou, T.; Morozov, S. V.; Grigorenko, A. N.; Geim, A. K.; Casiraghi, C.; Castro Neto, A. H.; Novoselov, K. S. Strong Light−Matter Interactions in Heterostructures of Atomically Thin Films. *Science* **2013**, *340*, 1311−1314.

(7) Chen, H.; Wen, X.; Zhang, J.; Wu, T.; Gong, Y.; Zhang, X.; Yuan, J.; Yi, C.; Lou, J.; Ajayan, P. M.; Zhuang, W.; Zhang, G.; Zheng, J. Ultrafast Formation of Interlayer Hot Excitons in Atomically Thin MoS_2/WS_2 Heterostructures. *Nat. Commun.* **2016**, *7*, 12510.

(8) Radisavljevic, B.; Radenovic, A.; Brivio, J.; Giacometti, i. V.; Kis, A. Single-Layer MoS_2 Transistors. *Nat. Nanotechnol.* **2011**, *6*, 147−150.

(9) Yin, Z.; Li, H.; Li, H.; Jiang, L.; Shi, Y.; Sun, Y.; Lu, G.; Zhang, Q.; Chen, X.; Zhang, H. Single-Layer MoS_2 Phototransistors. *ACS Nano* **2012**, *6*, 74−80.

(10) Zhang, W.; Huang, J. K.; Chen, C. H.; Chang, Y. H.; Cheng, Y. J.; Li, L. J. High-Gain Phototransistors Based on a CVD MoS_2 Monolayer. *Adv. Mater.* **2013**, *25*, 3456−3461.

(11) Perkins, F. K.; Friedman, A. L.; Cobas, E.; Campbell, P. M.; Jernigan, G. G.; Jonker, B. T. Chemical Vapor Sensing with Monolayer MoS2. *Nano Lett.* **2013**, *13*, 668−673.

(12) Bertolazzi, S.; Brivio, J.; Kis, A. Stretching and Breaking of Ultrathin MoS_2. *ACS Nano* **2011**, *5*, 9703−9709.

(13) Chang, H.-Y.; Yang, S.; Lee, J.; Tao, L.; Hwang, W.-S.; Jena, D.; Lu, N.; Akinwande, D. High-Performance, Highly Bendable MoS2 Transistors with High-K Dielectrics for Flexible Low-Power Systems. *ACS Nano* **2013**, *7*, 5446−5452.

(14) Novoselov, K. S.; Jiang, D.; Schedin, F.; Booth, T. J.; Khotkevich, V. V.; Morozov, S. V.; Geim, A. K. Two-Dimensional Atomic Crystals. *Proc. Natl. Acad. Sci. U. S. A.* **2005**, *102*, 10451.

(15) Coleman, J. N.; Lotya, M.; O'Neill, A.; Bergin, S. D.; King, P. J.; Khan, U.; Young, K.; Gaucher, A.; De, S.; Smith, R. J.; Shvets, I. V.; Arora, S. K.; Stanton, G.; Kim, H.-Y.; Lee, K.; Kim, G. T.; Duesberg, G. S.; Hallam, T.; Boland, J. J.; Wang, J. J.; Donegan, J. F.; Grunlan, J. C.; Moriarty, G.; Shmeliov, A.; Nicholls, R. J.; Perkins, J. M.; Grieveson, E. M.; Theuwissen, K.; McComb, D. W.; Nellist, P. D.; Nicolosi, V. Two-Dimensional Nanosheets Produced by Liquid Exfoliation of Layered Materials. *Science* **2011**, *331*, 568.

(16) Muratore, C.; Hu, J. J.; Wang, B.; Haque, M. A.; Bultman, J. E.; Jespersen, M. L.; Shamberger, P. J.; McConney, M. E.; Naguy, R. D.; Voevodin, A. A. Continuous Ultra-Thin MoS_2 Films Grown by Low Temperature Physical Vapor Deposition. *Appl. Phys. Lett.* **2014**, *104*, 261604.

(17) Zhan, Y.; Liu, Z.; Najmaei, S.; Ajayan, P. M.; Lou, J. Large-Area Vapor-Phase Growth and Characterization of MoS_2 Atomic Layers on A SiO_2 Substrate. *Small* **2012**, *8*, 966−971.

(18) Wang, X.; Feng, H.; Wu, Y.; Jiao, L. Controlled Synthesis of Highly Crystalline MoS_2 Flakes by Chemical Vapor Deposition. *J. Am. Chem. Soc.* **2013**, *135*, 5304−5307.

(19) Lee, Y. H.; Zhang, X. Q.; Zhang, W.; Chang, M. T.; Lin, C. T.; Chang, K. D.; Yu, Y. C.; Wang, J. T. W.; Chang, C. S.; Li, L. J.; Lin, T.-W. Synthesis of Large-Area MoS_2 Atomic Layers with Chemical Vapor Deposition. *Adv. Mater.* **2012**, *24*, 2320−2325.

(20) Wang, S.; Rong, Y.; Fan, Y.; Pacios, M.; Bhaskaran, H.; He, K.; Warner, J. H. Shape Evolution of Monolayer MoS_2 Crystals Grown by Chemical Vapor Deposition. *Chem. Mater.* **2014**, *26*, 6371−6379.

(21) van der Zande, A. M.; Huang, P. Y.; Chenet, D. A.; Berkelbach, T. C.; You, Y.; Lee, G.-H.; Heinz, T. F.; Reichman, D. R.; Muller, D. A.; Hone, J. C. Grains and Grain Boundaries in Highly Crystalline Monolayer Molybdenum Disulphide. *Nat. Mater.* **2013**, *12*, 554−561.

(22) Najmaei, S.; Liu, Z.; Zhou, W.; Zou, X.; Shi, G.; Lei, S.; Yakobson, B. I.; Idrobo, J.-C.; Ajayan, P. M.; Lou, J. Vapour Phase Growth and Grain Boundary Structure of Molybdenum Disulphide Atomic Layers. *Nat. Mater.* **2013**, *12*, 754−759.

(23) Yun, S. J.; Chae, S. H.; Kim, H.; Park, J. C.; Park, J.-H.; Han, G. H.; Lee, J. S.; Kim, S. M.; Oh, H. M.; Seok, J.; Jeong, M. S.; Kim, K. K.; Lee, Y. H. Synthesis of Centimeter-Scale Monolayer Tungsten Disulfide Film on Gold Foils. *ACS Nano* **2015**, *9*, 5510−5519.

(24) Gao, Y.; Liu, Z.; Sun, D.-M.; Huang, L.; Ma, L.-P.; Yin, L.-C.; Ma, T.; Zhang, Z.; Ma, X.-L.; Peng, L.-M.; Cheng, H.-M.; Ren, W. Large-Area Synthesis of High-Quality and Uniform Monolayer WS_2 on Reusable Au Foils. *Nat. Commun.* **2015**, *6*, 8569.
(25) Kang, K.; Xie, S.; Huang, L.; Han, Y.; Huang, P. Y.; Mak, K. F.; Kim, C.-J.; Muller, D.; Park, J. High-Mobility Three-Atom-Thick Semiconducting Films with Wafer-Scale Homogeneity. *Nature* **2015**, *520*, 656.
(26) Kim, H.; Ovchinnikov, D.; Deiana, D.; Unuchek, D.; Kis, A. Suppressing Nucleation in Metal-Organic Chemical Vapor Deposition of MoS_2 Monolayers by Alkali Metal Halides. *Nano Lett.* **2017**, *17*, 5056−5063.
(27) Shi, Y.; Yang, P.; Jiang, S.; Zhang, Z.; Huan, Y.; Xie, C.; Hong, M.; Shi, J.; Zhang, Y. Na-Assisted Fast Growth of Large Single-Crystal MoS_2 on Sapphire. *Nanotechnology* **2019**, *30*, No. 034002.
(28) Chen, J.; Zhao, X.; Grinblat, G.; Chen, Z.; Tan, S. J. R.; Fu, W.; Ding, Z.; Abdelwahab, I.; Li, Y.; Geng, D.; Liu, Y.; Leng, K.; Liu, B.; Liu, W.; Tang, W.; Maier, S. A.; Pennycook, S. J.; Loh, K. P. Homoepitaxial Growth of Large-Scale Highly Organized Transition Metal Dichalcogenide Patterns. *Adv. Mater.* **2018**, *30*, 1704674.
(29) Chen, J.; Zhao, X.; Tan, S. J. R.; Xu, H.; Wu, B.; Liu, B.; Fu, D.; Fu, W.; Geng, D.; Liu, Y.; Liu, W.; Tang, W.; Li, L.; Zhou, W.; Sum, T. C.; Loh, K. P. Chemical Vapor Deposition of Large-Size Monolayer $MoSe_2$ Crystals on Molten Glass. *J. Am. Chem. Soc.* **2017**, *139*, 1073−1076.
(30) Chen, W.; Zhao, J.; Zhang, J.; Gu, L.; Yang, Z.; Li, X.; Yu, H.; Zhu, X.; Yang, R.; Shi, D.; Lin, X.; Guo, J.; Bai, X.; Zhang, G. Oxygen-Assisted Chemical Vapor Deposition Growth of Large Single-Crystal and High-Quality Monolayer MoS_2. *J. Am. Chem. Soc.* **2015**, *137*, 15632−15635.
(31) Yang, P.; Zou, X.; Zhang, Z.; Hong, M.; Shi, J.; Chen, S.; Shu, J.; Zhao, L.; Jiang, S.; Zhou, X.; Huan, Y.; Xie, C.; Gao, P.; Chen, Q.; Zhang, Q.; Liu, Z.; Zhang, Y. Batch Production of 6-Inch Uniform Monolayer Molybdenum Disulfide Catalyzed by Sodium in Glass. *Nat. Commun.* **2018**, *9*, 979.
(32) Najmaei, S.; Amani, M.; Chin, M. L.; Liu, Z.; Birdwell, A. G.; O'Regan, T. P.; Ajayan, P. M.; Dubey, M.; Lou, J. Electrical Transport Properties of Polycrystalline Monolayer Molybdenum Disulfide. *ACS Nano* **2014**, *8*, 7930−7937.
(33) Van Der Koma, A. Waals Epitaxy for Highly Lattice-Mismatched Systems. *J. Cryst. Growth* **1999**, *201*, 236−241.
(34) Bakti Utama, M. I.; Zhang, Q.; Zhang, J.; Yuan, Y.; Belarre, F. J.; Arbiol, J.; Xiong, Q. Recent Developments and Future Directions in the Growth of Nanostructures by van der Waals Epitaxy. *Nanoscale* **2013**, *5*, 3570−3588.
(35) Ji, Q.; Kan, M.; Zhang, Y.; Guo, Y.; Ma, D.; Shi, J.; Sun, Q.; Chen, Q.; Zhang, Y.; Liu, Z. Unravelling Orientation Distribution and Merging Behavior of Monolayer MoS_2 Domains on Sapphire. *Nano Lett.* **2015**, *15*, 198−205.
(36) Chen, L.; Liu, B.; Ge, M.; Ma, Y.; Abbas, A. N.; Zhou, C. Step-Edge-Guided Nucleation and Growth of Aligned WSe2 on Sapphire via a Layer-over-Layer Growth Mode. *ACS Nano* **2015**, *9*, 8368−8375.
(37) Dumcenco, D.; Ovchinnikov, D.; Marinov, K.; Lazic, P.; Gibertini, M.; Marzari, N.; Sanchez, O. L.; Kung, Y.-C.; Krasnozhon, D.; Chen, M.-W.; Bertolazzi, S.; Gillet, P.; Morral, A. F. i.; Radenovic, A.; Kis, A. Large-Area Epitaxial Monolayer MoS_2. *ACS Nano* **2015**, *9*, 4611.
(38) Aljarb, A.; Cao, Z.; Tang, H.-L.; Huang, J.-K.; Li, M.; Hu, W.; Cavallo, L.; Li, L.-J. Substrate Lattice-Guided Seed Formation Controls the Orientation of 2D Transition-Metal Dichalcogenides. *ACS Nano* **2017**, *11*, 9215−9222.
(39) Suenaga, K.; Ji, H. G.; Lin, Y.-C.; Vincent, T.; Maruyama, M.; Aji, A. S.; Shiratsuchi, Y.; Ding, D.; Kawahara, K.; Okada, S.; Panchal, V.; Kazakova, O.; Hibino, H.; Suenaga, K.; Ago, H. Surface-Mediated Aligned Growth of Monolayer MoS_2 and In-Plane Heterostructures with Graphene on Sapphire. *ACS Nano* **2018**, *12*, 10032−10044.
(40) Wang, Q.; Li, N.; Tang, J.; Zhu, J.; Zhang, Q.; Jia, Q.; Lu, Y.; Wei, Z.; Yu, H.; Zhao, Y.; Guo, Y.; Gu, L.; Sun, G.; Yang, W.; Yang, R.; Shi, D.; Zhang, G. Wafer-Scale Highly Oriented Monolayer MoS_2 with Large Domain Sizes. *Nano Lett.* **2020**, *20*, 7193−7199.
(41) Ruzmetov, D.; Zhang, K.; Stan, G.; Kalanyan, B.; Bhimanapati, G. R.; Eichfeld, S. M.; Burke, R. A.; Shah, P. B.; O'Regan, T. P.; Crowne, F. J.; Birdwell, A. G.; Robinson, J. A.; Davydov, A. V.; Ivanov, T. G. Vertical 2D/3D Semiconductor Heterostructures Based on Epitaxial Molybdenum Disulfide and Gallium Nitride. *ACS Nano* **2016**, *10*, 3580−3588.
(42) Huang, J.-K.; Pu, J.; Hsu, C.-L.; Chiu, M.-H.; Juang, Z.-Y.; Chang, Y.-H.; Chang, W.-H.; Iwasa, Y.; Takenobu, T.; Li, L.-J. Large-Area Synthesis of Highly Crystalline WSe_2 Monolayers and Device Applications. *ACS Nano* **2014**, *8*, 923−930.
(43) Chen, P.; Xu, W.; Gao, Y.; Warner, J. H.; Castell, M. R. Epitaxial Growth of Monolayer MoS_2 on $SrTiO_3$ Single Crystal Substrates for Applications in Nanoelectronics. *ACS Appl. Nano Mater.* **2018**, *1*, 6976−6988.
(44) Yamamoto, M.; Einstein, T. L.; Fuhrer, M. S.; Cullen, W. G. Anisotropic Etching of Atomically Thin MoS_2. *J. Phys. Chem. C* **2013**, *117*, 25643−25649.
(45) Spychalski, W. L.; Pisarek, M.; Szoszkiewicz, R. Microscale Insight into Oxidation of Single MoS2 Crystals in Air. *J. Phys. Chem. C* **2017**, *121*, 26027−26033.
(46) Gulbransen, E. A.; Andrew, K. F.; Brassart, F. A. Oxidation of Molybdenum 550 ∼ to 1700∼ °C. *J. Electrochem. Soc.* **1963**, *110*, 952−959.
(47) Wang, R.; Guo, D.; Xie, G.; Pan, G. Atomic Step Formation on Sapphire Surface in Ultra-precision Manufacturing. *Sci. Rep.* **2016**, *6*, 29964.
(48) Curiotto, S.; Chatain, D. Surface Morphology and Composition of c-, a- and m-Sapphire Surfaces in O_2 and H_2 Environments. *Surf. Sci.* **2009**, *603*, 2688−2697.

https://doi.org/10.1021/acsanm.1c00469
ACS Appl. Nano Mater. 2021, 4, 4930−4938